Design and Proof-of-Concept of a Matrix Transducer Array for Clamp-on Ultrasonic Flow Measurements

Massaad, Jack; Van Neer, Paul L.M.J.; Van Willigen, Douwe M.; Noothout, Emile C.; De Jong, Nicolaas; Pertijs, Michiel A.P.; Verweij, Martin D.

DOI
10.1109/TUFFC.2022.3186170

Publication date
2022

Document Version
Accepted author manuscript

Published in
IEEE Transactions on Ultrasonics, Ferroelectrics, and Frequency Control

This article has been accepted for publication in IEEE Transactions on Ultrasonics, Ferroelectrics, and Frequency Control. This is the author's version which has not been fully edited and content may change prior to final publication. Citation information: DOI 10.1109/TUFFC.2022.3186170

Design and Proof-of-Concept of a Matrix Transducer Array for Clamp-on Ultrasonic Flow Measurements

Jack Massaad, *Graduate Student Member, IEEE,* Paul L. M. J. van Neer, Douwe M. van Willigen, *Graduate Student Member, IEEE,* Emile C. Noothout, Nicolaas de Jong, *Member, IEEE,* Michiel A. P. Pertijs, *Senior Member, IEEE,* and Martin D. Verweij, *Member, IEEE*

Abstract

Common clamp-on ultrasonic flow meters consist of two single-element transducers placed on the pipe wall. Flow speed is measured non-invasively, i.e. without interrupting the flow and without perforating the pipe wall, which also minimizes safety risks and avoids pressure drops inside the pipe. However, before metering, the transducers have to be carefully positioned along the pipe axis to correctly align the acoustic beams and obtain a well-calibrated flow meter. This process is done manually, is dependent on the properties of the pipe and the liquid, does not account for pipe imperfections, and becomes troublesome on pipelines with an intricate shape. Matrix transducer arrays are suitable to dynamically steer acoustic beams and realize self-alignment upon reception, without user input. In this work, the design of a broadband 37x17 matrix array (center frequency of $1\,\mathrm{MHz}$) to perform clamp-on ultrasonic flow measurements over a wide range of liquids ($c = 1000 - 2000\,\mathrm{m/s}$, $\alpha \leq 1\,\mathrm{dB/MHz.cm}$) and pipe sizes is presented. Three critical aspects were assessed: efficiency, electronic beam steering, and wave mode conversion in the pipe wall. A prototype of a proof-of-concept flow meter consisting of two 36-element linear arrays (center frequency of $1.1\,\mathrm{MHz}$) was fabricated and placed on a $1\,\mathrm{mm}$-thick, $40\,\mathrm{mm}$-inner diameter stainless steel pipe in a custom-made flow loop filled with water. At resonance, simulated and measured efficiencies in water of the linear arrays compared well: $0.88\,\mathrm{kPa/V}$ and $0.81\,\mathrm{kPa/V}$, respectively. Mean flow measurements were achieved by electronic beam steering of the acoustic beams and using both compressional and shear waves generated in the pipe wall. Correlation coefficients of $R^2 > 0.99$ between measured and reference flow speeds were obtained, thus showing the operational concept of an array-based clamp-on ultrasonic flow meter.

Index Terms

beam steering, clamp-on flow meter, ultrasound flow meter, Guided waves, transducer design.

This work is part of the research programme FLOW+, which is financed by the Dutch Technology Foundation STW (project 15031) and industrial partners Bronkhorst and KROHNE.

J. Massaad, P. L. M. J. van Neer, E. C. Noothout, N. de Jong, and M. D. Verweij are with the Laboratory of Medical Imaging, Faculty of Applied Sciences, Delft University of Technology, 2628CJ Delft, The Netherlands. (e-mail: J.M.MassaadMouawad@tudelft.nl).

D. M. van Willigen, and M. A. P. Pertijs are with the Electronic Instrumentation Laboratory, Faculty of Electrical Engineering, Mathematics and Computer Science, Delft University of Technology, 2628CD Delft, The Netherlands. (e-mail: D.M.vanWilligen@tudelft.nl).

P. L. M. J. van Neer is also with the Department of Acoustics and Sonar, TNO, 2597AK, The Hague, The Netherlands. (e-mail: paul.vanneer@tno.nl).

M. D. Verweij, and N. de Jong are also with the Department of Biomedical Engineering, Thorax Center, Erasmus MC, 3015GD, Rotterdam, The Netherlands. (e-mail: M.D.Verweij@tudelft.nl).

This article has been accepted for publication in IEEE Transactions on Ultrasonics, Ferroelectrics, and Frequency Control. This is the author's version which has not been fully edited and content may change prior to final publication. Citation information: DOI 10.1109/TUFFC.2022.3186170

Design and Proof-of-Concept of a Matrix Transducer Array for Clamp-on Ultrasonic Flow Measurements

I. Introduction

Ultrasonic flow meters are used in a wide range of industrial applications [1]–[3], and can be divided in two categories: in-line and clamp-on. Clamp-on flow meters consist of two angled, single-element transducers fixed along the outside of a pipe wall. Alternately, each transducer emits an ultrasound wave which is transmitted through the pipe wall and refracted into the liquid, where it can bounce one or more times before refracting back into the pipe wall and being received by the other transducer. The transit time difference between the signals recorded upstream and downstream is proportional to the flow speed [4], at least for small flow velocities.

Clamp-on flow meters have advantages compared to their in-line counterparts with transducers fixed inside the pipe wall. They can be installed without interruption of the flow and without the addition of extra pipe sections or making cuts through existing ones. Nevertheless, clamp-on flow meters also have disadvantages. Obtaining a predetermined spacing between the transducers requires a priori knowledge of the properties and geometry of the pipe, as well as the speed of sound in the liquid is needed. In practice, these values are not exactly known and this limits the accuracy of the calibration and, consequently, the measurements. Alternatively, the transducers can be spaced using a manual positioning procedure, which is cumbersome, labour intensive and operator dependent.

Common clamp-on flow meters use a specific wave type in the pipe wall (typically a bulk shear wave, but in principle this may also be a bulk compressional wave). This wave will refract into the fluid to obtain information about the flow speed. However, it also excites Lamb waves in the pipe wall. These Lamb waves interfere with the compressional wave refracting back from the liquid and introduce an offset error in the transit time differences and hence in the measurement of the corresponding flow speed. To tackle this issue, current clamp-on flow meters may incorporate an absorbing layer placed around the pipe wall and in-between both transducers with the purpose of attenuating these interfering Lamb waves [5]. Unfortunately, this solution is not always practical, as access to the pipe is often limited, and/or the pipe is covered by material with other purposes, e.g. heat isolation. Other solutions for dealing with Lamb waves in the pipe wall consist in modifying the angle of the wedge that forms the coupling between the transducer and the pipe wall, or the resonance frequency of the transducer, or both. Ultimately, either solution also requires manual displacement of the transducers on the pipe wall, thus keeping the process operator-dependent.

A pair of matrix transducer arrays has the potential to tackle the current problems and limitations of clamp-on flow meters. Prior to flow measurements, with these transducers the properties of the pipe and the liquid, such as bulk wave sound speeds and pipe diameter can be obtained using dedicated measurements, and the measured parameters can be combined with electronic beam steering capabilities to create a self-calibrated flow sensor [6], [7]. Furthermore, the transducer arrays can be cleverly excited to suppress, in transmission, the spurious Lamb waves in the pipe wall while maintaining a beam shape in the liquid with a clearly defined flat wavefront [8].

The techniques mentioned in the previous paragraph are new in the context of clamp-on ultrasonic flow metering and, in principle, require no input from the operator and no manual positioning to improve measurement accuracy. In this context, measurement accuracy is defined as the proximity of a measured flow speed value to the true flow speed value (i.e. the one reported by a reference flow meter). Most of the currently available clamp-on ultrasonic flow meters claim an accuracy no better than $97\,\%$ [1], while the best ones are able to reach an accuracy above $98\,\%$ [9].

There exists previous work on using transducer arrays to measure flow [10]–[18]. However, these array-based solutions describe an in-line configuration of the sensors. In [19], a study is presented on the manufacturing feasibility of low-frequency arrays made of fiber-reinforced polymer composites placed outside a rectangular duct for gas flow metering. In the current work, a matrix transducer array for clamp-on ultrasonic flow metering within a wide range of liquid and pipe parameters is proposed. An acoustic stack is presented, and a detailed explanation is given for the choices that were made. Moreover, the purpose of this paper is to show a proof-of-concept of a functioning sensor by focusing on three critical aspects: efficiency (i.e. transmit transfer function of the array), electronic beam steering, and wave mode conversion in the pipe wall. The proof-of-concept consists of flow measurements with a prototype based on two custom-made linear transducer arrays, and shows the feasibility of transducer array-based clamp-on ultrasonic flow meters.

II. Conventional and Matrix Clamp-on Ultrasonic Flow Meters

Consider two single-element transducers, with a wedge with angle θ, placed on the outer pipe wall with a center-to-center axial separation x, as shown in Fig. 1a. The angled wedge

This article has been accepted for publication in IEEE Transactions on Ultrasonics, Ferroelectrics, and Frequency Control. This is the author's version which has not been fully edited and content may change prior to final publication. Citation information: DOI 10.1109/TUFFC.2022.3186170

allows the compressional wave generated by the transducers to impinge the pipe wall under a certain angle with respect to the normal of the pipe surface. At the interface between the wedge and the pipe wall, wave mode conversion occurs, i.e. a compressional and a shear wave get excited in the pipe wall. Then, at the interface between the pipe wall and the liquid, wave mode conversion takes places again. Here, both waves in the pipe wall refract into the liquid as compressional waves. Given the sound speeds of common metal pipe walls and of common liquids, Snell's law predicts that shear waves in the pipe wall refract under higher angles into the liquid compared to compressional waves in the pipe wall. For this reason, common clamp-on ultrasonic flow meters use wedges with sufficiently-high angles to only excite shear waves in the pipe wall (the compressional waves will be evanescent), so that the longest horizontal path in the fluid is obtained and, consequently, the highest possible sensitivity of the acoustic wave to the flow is achieved. However, during propagation over such long travel paths, the beam also experiences more attenuation compared to shorter travel paths. The compressional wave propagating in the liquid may reflect a few times within the pipe before finally refracting back into the pipe wall and reaching the other transducer. This procedure occurs both upstream and downstream, and given that the flow velocity adds up vectorially to the velocity of the wave in the liquid, both signals will be recorded with a transit time difference that will finally be proportional to the desired flow speed, at least for flow speeds well below the wave speed in the fluid.

To make an accurate flow measurement, the distance x must be adjusted correctly, otherwise, the incoming flow-sensitive wave does not reach the receiving transducer (Fig. 1a). Also, in practice, other waves such as the one reflected by the outer surface of the pipe wall, may also occur. Thus, the distance x is chosen such that the incoming flow-sensitive wave may be selected through time windowing. The distance x depends on the angle of the wedge, the bulk wave sound speeds of the pipe wall, the pipe wall thickness, the pipe diameter, the sound speed of the liquid, and also on the number of bounces inside the pipe. In practice, the distance x is found by fixing one of the transducers and manually moving the other one along the pipe wall until a peak amplitude is detected. This results in a cumbersome and time-consuming process for the operator, especially in hardly accessible places. Moreover, most of the parameters required for calibration are not exactly known and the procedure doesn't account for pipe imperfections (e.g. variations of pipe wall thickness and diameter, effects of corrosion). A clamp-on ultrasonic flow meter based on two matrix arrays (for one array, see Fig. 1b) offers beam steering capabilities that can be applied to exactly aim at the receiving transducer without the need of manual positioning, and could also be used to measure the parameters of the pipe and the liquid [6], [7] that are required for proper calibration.

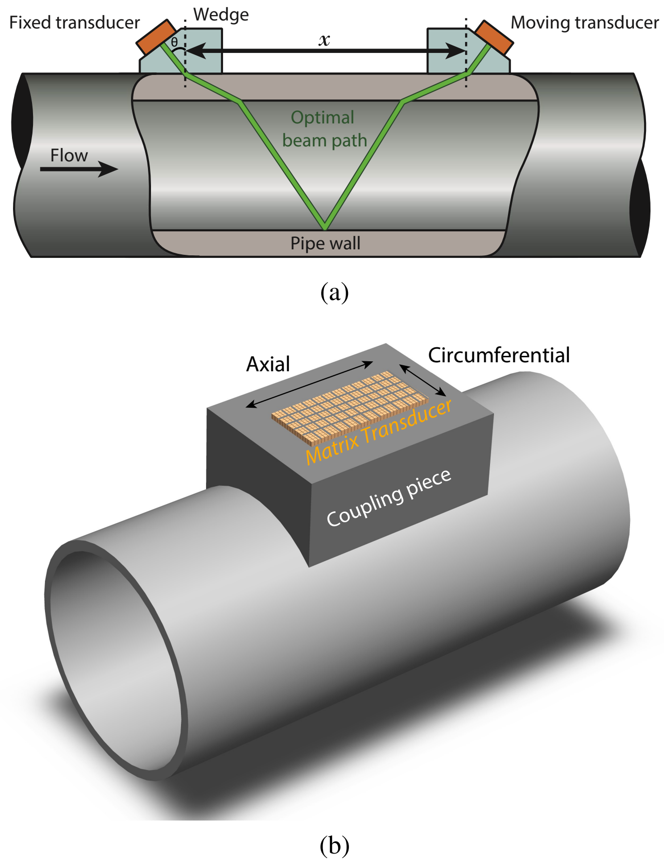

Figure 1: (a) Sketch of a conventional clamp-on ultrasonic flow meter. Upon installation, one single-element transducer is manually moved along the pipe wall to find the optimal distance x, which depends on the properties and geometry of the pipe wall, and on the sound speed of the liquid. The green line represents the path of the flow-sensitive wave. Here the wave bounces only once inside the pipe. For clarity, the travel paths of other waves are not shown. (b) Concept of a matrix transducer array for clamp-on ultrasonic flow metering, with array elements along the axial and the circumferential direction.

III. Basic Requirements

A. Parameter Ranges of Liquid and Pipe

Because of the wide range of liquids used in practice, our sensor should be able to measure the flow of liquids with sounds speed ranging from $c_{\text{liquid}} = 1000 - 2000\,\text{m/s}$, and attenuation coefficients $\alpha \leq 1\,\text{dB/MHz.cm}$ [20].

Most pipes in industrial applications are made of steel, and corresponding material properties are considered in this work. The sensor should operate on pipes with inner diameters ranging from $25 - 100\,\text{mm}$. Next to that, a wide range of pipe wall thicknesses occurs in practice, therefore our sensor should be able to deal with pipe wall thicknesses ranging from $1 - 5\,\text{mm}$.

B. Minimum Signal-to-Noise Ratio

Current clamp-on ultrasonic flow meters perform flow measurements with a single-shot signal-to-noise ratio (SNR) as low as $20\,\text{dB}$. Therefore, it is our aim to obtain a flow meter design that produces this minimum value of SNR within the desired frequency range and for all considered liquids.

IV. Matrix Array design

The sensor proposed in this section was designed by partially following the methodologies described in [8], [21].

A. Acoustic Stack

In Fig. 2a, a cross-section of the acoustic stack of the designed matrix transducer array is shown along the axial direction, and in Fig. 2b, its modeled transfer functions are shown. The stack was designed using the Finite Element software package PZFlex (Onscale, Redwood City, CA, USA). The acoustic stack consists of an $11\,\mathrm{mm}$-thick lead coupling layer, 37 $1.24\,\mathrm{mm}$-thick piezo-elements made of HK1HD (TRS Technologies, Inc., State College, PA), a $1.6\,\mathrm{mm}$-thick Printed Circuit Board (PCB) layer, and a $40\,\mathrm{mm}$-thick backing layer. The PCB layer also included $200\,\mu\mathrm{m}$-wide air vias centered on the electrode of each piezo-element. The walls of these vias were covered by a $20\,\mu\mathrm{m}$-thick copper layer. A backing material with the same acoustic impedance as the PCB layer ($6.7\,\mathrm{MRayl}$) and an attenuation coefficient of $5\,\mathrm{dB/MHz.cm}$ was placed on top to maximize the attenuation of the backward propagating waves. This was a relatively soft backing material, and its attenuation coefficient was based on practical experience with these kinds of materials. Other ultrasound applications, such as medical imaging, aim to attenuate the waves in the backing by $\approx 40\,\mathrm{dB}$ after a two-way travel path through its thickness. Based on this, the same level of damping was aimed for in our application. Hence, the thickness of the backing layer was set to $40\,\mathrm{mm}$. In the Appendix, Tables I and II report the properties of the materials used in FEM simulations of the acoustic stack shown in Fig. 2a, and Table III reports their dimensions.

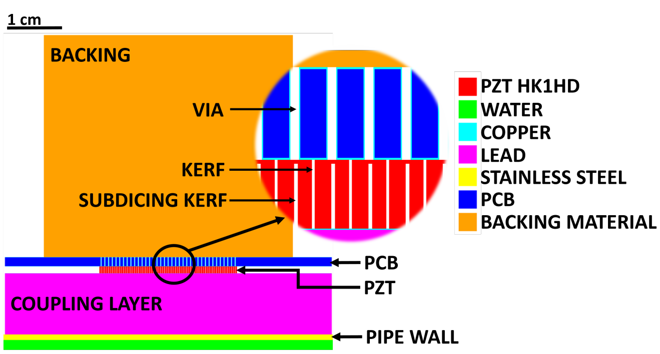

(a)

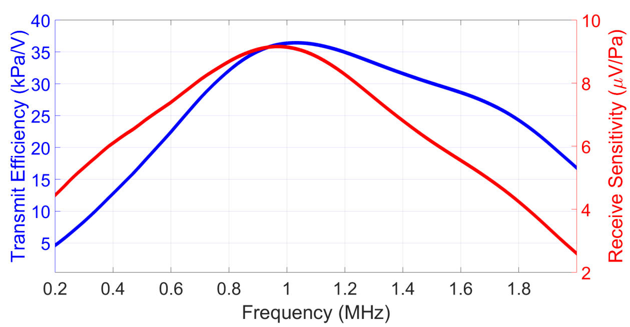

(b)

Figure 2: (a) Acoustic stack of the designed transducer array. The subdices of the PZT elements run up to $95\,\%$ of the element thickness. (b) Expected performance of the designed transducer array. There are no modes with lateral vibrations within the frequency band of interest ($0.2-2\,\mathrm{MHz}$). Both the transmit efficiency and the receive sensitivity were computed at the interface between the piezo-elements and the lead.

B. Center Frequency and Bandwidth

The center frequency (thickness resonance mode) of the designed matrix array was $1\,\mathrm{MHz}$, located within an operational frequency band ranging from $0.2\,\mathrm{MHz}$ to $2\,\mathrm{MHz}$ (see Fig. 2b), which covers the range of center-frequencies for typical ultrasonic flow meters [1]. Usually, transducers with a relatively low center-frequency are used for measuring the most attenuating liquids or in pipes with a large diameter relative to the wavelength, and transducers with a relatively high center-frequency are used in pipes with a small diameter.

1) Thickness of Piezo Elements: Each acoustic layer shown in Fig. 2a influences the whole resonance system and the resonance frequencies of the acoustic stack. Thus, with the addition of each layer, the thickness of the piezo-elements was modified accordingly, resulting in a final thickness value of $1.24\,\mathrm{mm}$, which differs slightly from the commonly expected $\lambda/4$ thickness (i.e. $\approx 1.03\,\mathrm{mm}$ at $1\,\mathrm{MHz}$).

2) Signal-to-Noise Ratio (SNR): Using the Johnson-Nyquist equation to calculate thermal noise [21], it was estimated that the average RMS noise level of the piezo-elements would be in the order of $1.1\,\mu\mathrm{V}$. This would be the noise level in the best case scenario, i.e. when noise from the rest of the equipment is negligible. This noise level, in combination with the SONAR equation [21], was used to compute the expected SNR levels of the designed array both in case of compressional waves and in case of shear waves in the pipe wall. Fig. 3 shows the expected SNR levels, where at resonance (i.e. $1\,\mathrm{MHz}$), SNR $\geq 20\,\mathrm{dB}$ for all considered liquids, satisfying the basic requirements defined in Section III.

C. Pitch

To enable spatial filtering and beam steering, the matrix array should be properly spatially sampled, i.e. have a sufficiently small pitch. To ensure this, Lamb wave modes of the thickest considered stainless steel pipe wall ($5\,\mathrm{mm}$) were analyzed. From this study, the pitch was set to $0.72\,\mathrm{mm}$, which is half the wavelength of the slowest propagating Lamb wave mode at a frequency of $2\,\mathrm{MHz}$ ($c_{\mathrm{low}} = 2900\,\mathrm{m/s}$).

The piezo-elements were subdiced up to $95\,\%$ of their thickness, as shown in Fig. 2a. The width of the sub-dicing kerf was $50\,\mu\mathrm{m}$, which is the same as for the kerfs of the array. This ensured the shift of lateral resonance modes to frequencies of, at least, $3\,\mathrm{MHz}$, i.e. outside our bandwidth of interest [22].

D. Coupling Piece

Current clamp-on ultrasonic flow meters excite shear waves in the pipe wall to achieve higher refraction angles in the

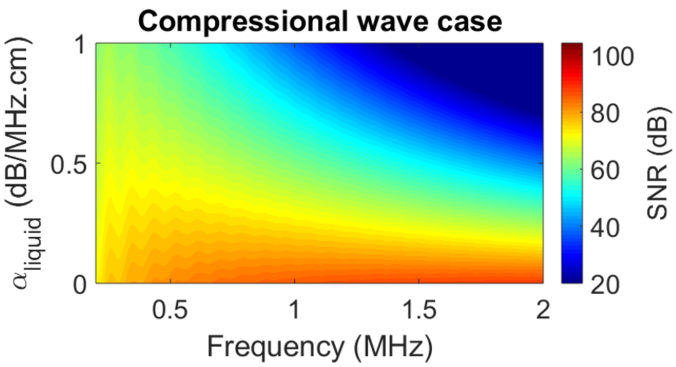

(a)

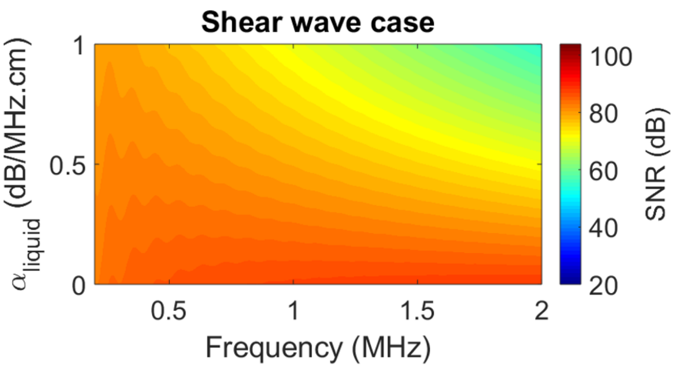

(b)

Figure 3: Computed SNR of the designed transducer array, versus frequency and attenuation coefficient of the liquid. (a) Compressional waves in the pipe wall and six bounces (v-shapes) of the acoustic beam within the pipe. (b) Shear waves in the pipe wall and two bounces (v-shapes) of the acoustic beam within the pipe.

liquids, and therefore improve beam sensitivity to the flow. The way to excite such waves is by impinging a compressional wave on the pipe wall beyond the critical angle for the refracted compressional wave. To obtain shear waves in the pipe wall at sufficiently high incidence angles, plastic wedges with a much lower compressional sound speed are commonly placed between the transducer and the pipe wall.

Nevertheless, the acoustic impedance of plastic ($Z_{\text{wedge}} \approx 2.5\,\text{MRayl}$) relative to that of the metal pipe wall ($Z_{wall} \approx 47\,\text{MRayl}$) leads to a low transmission coefficient since most of the impinging energy gets reflected back into the wedge. Therefore, in our case it was necessary to consider a coupling material that had roughly the same compressional sound speed as plastic ($c_{\text{plastic}} = 2290\,\text{m/s}$) to achieve wave mode conversion at reasonably high incidence angles, but a much higher density than plastic ($\rho_{\text{plastic}} = 1.24\,\text{kg/m}^3$) to achieve an impedance closer to steel and get sufficient energy into the pipe wall. These parameters were the motivation to choose lead ($c_L = 2200\,\text{m/s}$, $\rho = 11200\,\text{kg/m}^3$) as the coupling material between the transducer array and the pipe wall.

The flat upper surface of our coupling piece runs parallel to the pipe wall in the axial direction, i.e. the coupling piece is not an angled wedge, and the lower surface conforms to the pipe wall. The thickness of the lead piece was set to $11\,\text{mm}$ at the center, and thicker towards the edges in the circumferential direction. This thickness allowed for time-windowing of the generated time pulses.

Nowadays, there is a clear drive to avoid lead in products. In practice, another coupling material should be used. However, in this work a novel concept is presented for scientific purposes, and no effort was paid to find an alternative material.

E. Aperture Size: Number of Array Elements

There are several factors that affect the accuracy and precision of clamp-on ultrasonic flow meters. The most common ones are: the input voltage over the transducer clamps, the input pulse type/shape, the system noise in reception, and crosstalk. The crosstalk has an electrical and an acoustical component. Acoustical crosstalk consists of spurious guided waves that propagate within the pipe wall, which interfere with the compressional wave that refracts from the liquid, introducing an offset in the transit time differences, thus affecting the accuracy of the flow speed measurement. Spurious guided waves are coherent and synchronized in time with the excitation signals, hence their effects cannot be reduced by averaging in the time domain. Also, the generation of spurious guided waves cannot be avoided by placing the transducers somewhere else on the pipeline. As mentioned in Section I, these waves may not always be windowed-out in the time domain, and placing absorbing layers around the pipe may not always be possible. Thus, it was assumed that spurious guided waves are the main factor that limit measurement accuracy of clamp-on ultrasonic flow meters. The method proposed in [8] was used to define the matrix array aperture, in both axial and circumferential direction, to achieve a $99\,\%$ measurement accuracy. This first required to find how much these guided waves need to be suppressed to achieve this accuracy.

A study was performed, in which two harmonic 'clean' waveforms, representing upstream and downstream signals in a flow measurement, were phase-shifted by a known amount, which was later retrieved with a cross-correlation algorithm implemented in the Fourier domain. In this domain, a rectangular windowed harmonic wave yields spurious oscillations (Gibb's phenomenon), which in combination with noise may result in a shift of the peak of the cross-correlation function from the correct place, thus causing an error in the estimation of the phase-shift between the upstream and the downstream signals. To minimize this error, signals with much lower spurious oscillations were used, specifically 5-cycle Gaussian-modulated sine waves with a center frequency of $f_c = 1\,\text{MHz}$. A linear relationship was obtained between the imposed phase-shift and the phase-shift computed by cross-correlation, as expected. However, when a spurious signal (now being a continuous sine wave with a center frequency of $f_c = 1\,\text{MHz}$) was added to the 'clean' waveforms, this relation was not linear anymore since the spurious signals introduce an offset error in the relative phase-shift between upstream and downstream signals. A nonlinear relation between the amplitude of the spurious wave and the induced phase shift error was obtained. As Fig. 4 shows, the induced error increases when the amplitude of the spurious wave increases.

This article has been accepted for publication in IEEE Transactions on Ultrasonics, Ferroelectrics, and Frequency Control. This is the author's version which has not been fully edited and content may change prior to final publication. Citation information: DOI 10.1109/TUFFC.2022.3186170

Considering transducer separations larger than $5\,\mathrm{cm}$ along the axial direction, and a $99\,\%$ measurement accuracy, the computed transit time differences were translated into an amplitude of a spurious wave mode via the relation shown in Fig. 4, and it was found that the amplitudes of the Lamb waves needed to be $55\,\mathrm{dB}$ below the amplitude of the compressional wave refracting from the liquid.

1) Number of Elements along Axial Direction: Finite Element simulations using PZFlex were performed for a clamp-on flow measurement setting (Fig. 5a), assuming a liquid with the highest considered attenuation ($\alpha = 1\,\mathrm{dB/MHz.cm}$). The transducer array was simulated to generate a steered acoustic beam. For this case it was found that Lamb waves have amplitude levels that are $20\,\mathrm{dB}$ below the amplitude of the compressional wave that refracts from the liquid (Fig. 5b). According to the previous paragraph, it was therefore necessary to further suppress the Lamb waves by $35\,\mathrm{dB}$.

Because our flow sensor consists of transducer arrays, several signal processing techniques based on phase-shift and amplitude manipulation of the element signals could be exploited to suppress the generated Lamb waves in transmission [23]–[26]. Unfortunately, the element phases required for this suppression would add to the element phases required for beam steering, which would result in a significantly deformed acoustic beam. Therefore, it was decided to manipulate the element amplitudes, i.e. apply apodization, for Lamb wave suppression and use the element phase shifts for beam steering and focusing. This method was described in [8], where it was concluded that, for an array satisfying the given requirements, 37 piezo-elements were enough to generate an acoustic wave with a sufficiently smooth beam profile to achieve $35\,\mathrm{dB}$ suppression of the Lamb waves along the axial direction. At the same time, upon reception a beam having the same width as the receiving array aperture was obtained, which maximizes SNR during flow measurements.

2) Number of Elements along Circumferential Direction: It was desired to use the matrix arrays to also compute the pipe diameter using the method proposed in [7], which consists in measuring the Lamb waves that propagate in the circumferential direction of the pipe wall. To achieve this, it was assumed that the sound speed of two guided waves propagating in two opposite directions across the circumference of the pipe wall should be measured within an error of $1\,\mathrm{m/s}$. For a pipe with the same dimensions as the one shown in Fig. 5a, this translated into a transit time difference of approx. $29\,\mathrm{ns}$ (i.e. a phase shift error of $0.18\,\mathrm{rad}$ considering a center frequency of $1\,\mathrm{MHz}$). Using the nonlinear relation of Fig. 4, this value ultimately translated into an amplitude of 0.08 (i.e. $22\,\mathrm{dB}$) for the spurious wave that needs to be suppressed. Knowing this, the method described in [8] predicted that 17 elements were enough to measure the pipe diameter and the flow speed with the required accuracy.

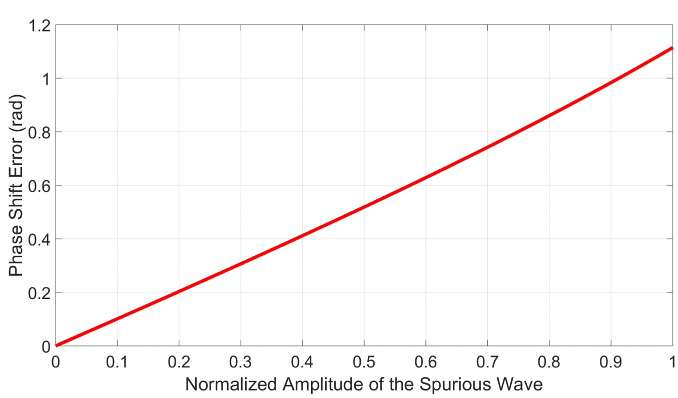

Figure 4: Nonlinear phase-shift error induced by spurious signals, versus the normalized amplitudes of these spurious signals. Amplitude is normalized to the maximum amplitude of the 'clean' upstream and downstream signals.

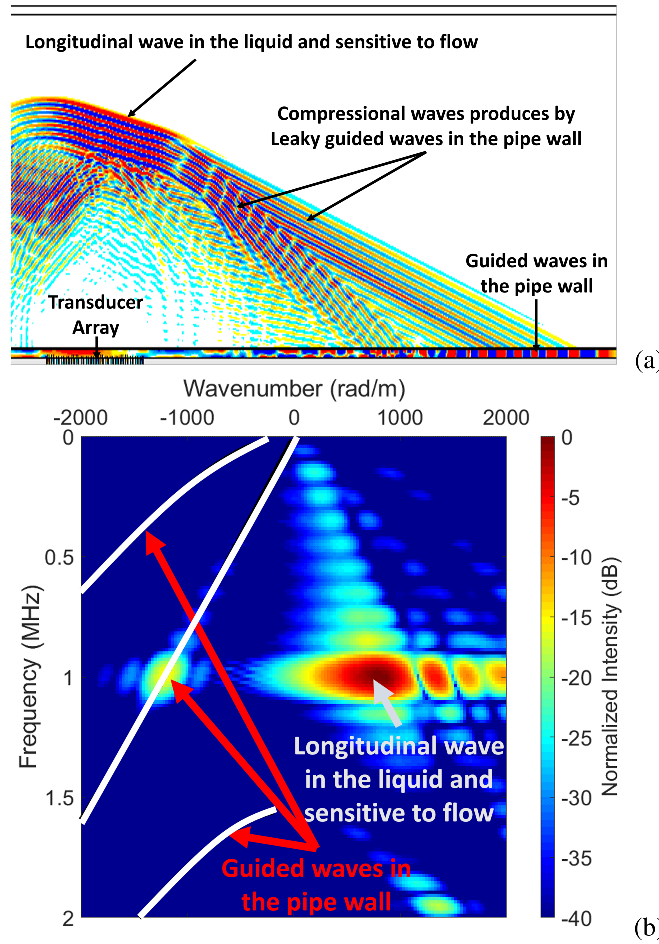

Figure 5: (a) Finite Element simulation of the acoustic field generated by a transducer array with beam steering, located on the bottom side of a $1\,\mathrm{mm}$-thick stainless steel pipe with an inner diameter of $40\,\mathrm{mm}$ and filled with a fluid with $c_{\mathrm{liquid}} = 1500\,\mathrm{m/s}$ and $\alpha = 1\,\mathrm{dB/MHz.cm}$. (b) Magnitude in the wavenumber-frequency domain of the narrow-banded time signals recorded along the bottom pipe wall (i.e. along the same surface on which the array is located) of the geometry in (a). The guided waves in the pipe wall have approximately $20\,\mathrm{dB}$ lower amplitude relative to the compressional wave that is refracted from the flow. The white lines represent the theoretical dispersion curves of the guided waves in the pipe wall.

This article has been accepted for publication in IEEE Transactions on Ultrasonics, Ferroelectrics, and Frequency Control. This is the author's version which has not been fully edited and content may change prior to final publication. Citation information: DOI 10.1109/TUFFC.2022.3186170

F. Axial Positioning on the Pipe Wall

To measure flow for liquids with $c_{\text{liquid}} = 1000 - 2000\,\text{m/s}$ and $\alpha \leq 1\,\text{dB/MHz.cm}$, it was necessary to determine the appropriate axial separation between both transducer arrays. This value was found via ray tracing. Assuming compressional waves in the pipe wall and six bounces (v-shapes) of the beam in the liquid (Fig. 6a), and assuming shear waves in the pipe wall and two bounces of the beam in the liquid (Fig. 6b), it was found that an axial transducer separation (i.e. center-to-center distance) of $80\,\text{mm}$ would make it possible to measure flow in both scenarios for the entire range of liquids considered, avoiding at the same time the critical angles for which the axial travel distance goes to infinity (see Fig. 6c). Moreover, at this axial transducer separation, the acoustic beam width at the $-3\,\text{dB}$ level ($26.1\,\text{mm}$) was almost the same as the array aperture along the axial direction of the pipe ($26.6\,\text{mm}$) [8].

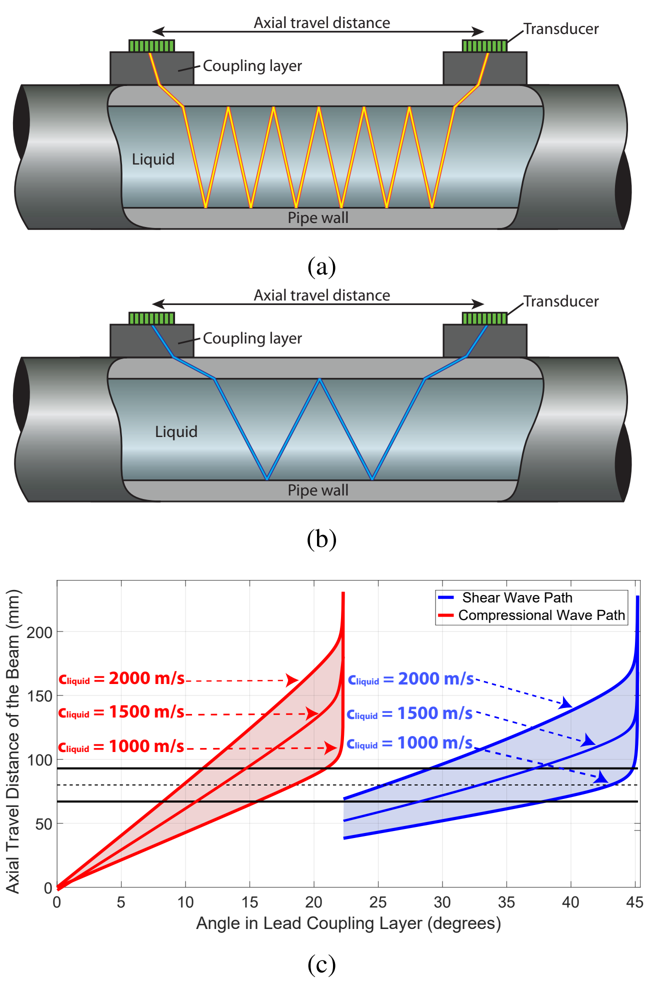

Figure 6: Travel path of an acoustic beam during clamp-on ultrasonic flow measurements using (a) compressional, and (b) shear waves in the pipe wall. (c) Axial travel distance of the beam (equal to the axial transducer separation) versus the beam angle in the coupling layer, for a pipe with an inner diameter of $40\,\text{mm}$. The black dashed line represents the physical location of the center of the receiver transducer array ($80\,\text{mm}$), and the black solid lines give the boundaries of its aperture in the axial direction.

V. Proof-of-Concept Prototype Based on a Linear Array

To test the potential performance of the proposed flow sensor without dealing with the complexity of making matrix arrays, we identified three critical aspects to be assessed with a proof-of-concept: efficiency, electronic beam steering, and wave mode conversion in the pipe wall. These parameters can be investigated with linear arrays, for which we fabricated two prototypes. Moreover, a prototype flow sensor, consisting of these linear arrays mounted on a stainless steel pipe section, was used to perform flow speed measurements in a custom-made flow loop.

A. Fabrication

Despite the superior results obtained using the $1.24\,\text{mm}$-thick HK1HD PZT material, due to lengthy delivery times two $1.67\,\text{mm}$-thick plates of PZ26 (Meggit A/S, Kvistgård, DK) were used to fabricate 36-element linear arrays. The choice of number of array elements was made to have a simple design of the electronics hardware. In the azimuthal direction, each array element had a width of $0.62\,\text{mm}$, and a kerf of $0.1\,\text{mm}$. In the elevational direction, each element had a height of $12\,\text{mm}$ (i.e. $\approx 17\text{x}0.72\,\text{mm}$).

In addition, a backing material was fabricated. It consisted of a mix of epoxy and tungsten particles of different sizes. The backing had an acoustic impedance of $Z \approx 6.7\,\text{MRayl}$, and an attenuation coefficient at $1\,\text{MHz}$ of $\alpha \approx 15\,\text{dB/MHz.cm}$. Therefore, a $13\,\text{mm}$-thick backing was sufficient to achieve a $40\,\text{dB}$ attenuation over the two-way travel path of the waves reflecting at the backside of this layer.

Molten lead was poured into custom-made molds to fabricate the desired coupling pieces. To characterize the array, a flat $11\,\text{mm}$ thick lead piece was cast. For performing the flow measurements, pieces with a concave shape were made that would fit on top of a stainless steel pipe with an outer diameter of $42\,\text{mm}$. This piece had a minimum thickness of $11\,\text{mm}$ in its center.

Figure 7 shows the prototype of fabricated linear array, including the array after the dicing process. In the Appendix, Table IV reports the dimensions of each layer. To acoustically characterize a single array, an experimental setup was built, consisting of the fabricated array coupled to a $1\,\text{mm}$-thick stainless steel plate and subsequently placed in water.

B. Transmit Transfer Function

All array elements were excited with a rectangular pulse using a Verasonics V1 system (Verasonics Inc., Kirkland, WA, USA). A peak transmit voltage of $V_{\text{tr}} = 5\,\text{V}$ was used. Measurements of the acoustic wavefield were performed with a hydrophone with $0.2\,\text{mm}$ diameter (Precision Acoustics Ltd., Dorchester, UK). These were used to measure the transmit transfer function of the array via the following equation [27]

$$T_{\text{t}}(\omega) = \frac{V_{\text{rc}}(\omega)}{V_{\text{tr}}(\omega)D(\omega)T_{\text{amp}}(\omega)T_{\text{hyd}}(\omega)}, \tag{1}$$

This article has been accepted for publication in IEEE Transactions on Ultrasonics, Ferroelectrics, and Frequency Control. This is the author's version which has not been fully edited and content may change prior to final publication. Citation information: DOI 10.1109/TUFFC.2022.3186170

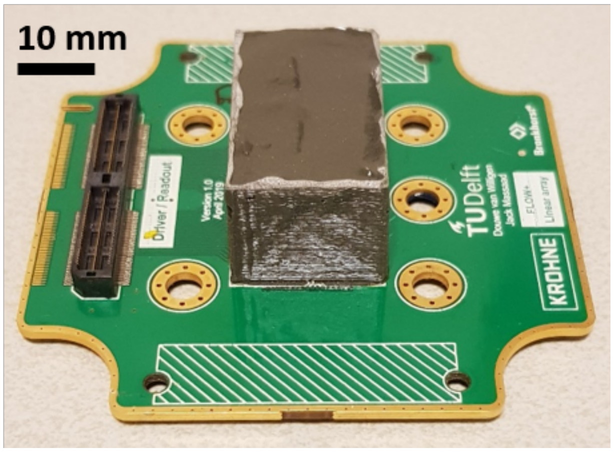

(a)

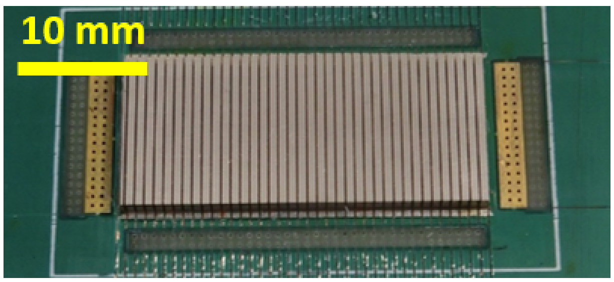

(b)

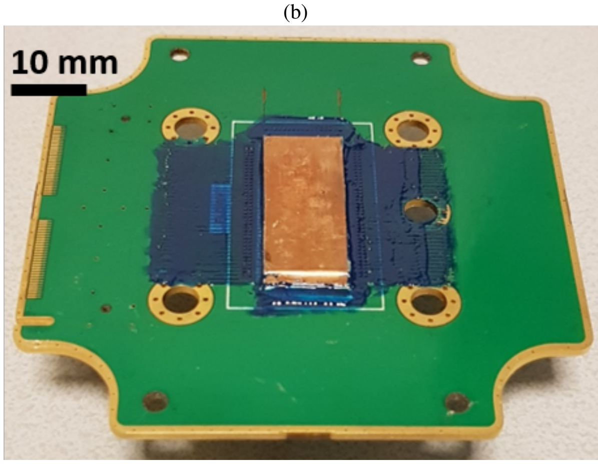

(c)

Figure 7: Fabricated prototype of one of the linear arrays. (a) Backing poored on top of the custom-made PCB. (b) Array obtained after dicing the PZ26 plate on top of the PCB and before applying a copper ground foil. (c) PZT array with a $20\,\mu\mathrm{m}$ thick copper ground foil layer.

where ω represents the angular frequency, $V_{\mathrm{tr}}(\omega)$ represents the Fourier transform of the transmitted time signal, and $V_{\mathrm{rc}}(\omega)$ represents the Fourier transform of the signal measured by the hydrophone. The symbol $D(\omega)$ represents the diffraction correction of the acoustic wavefield, $T_{\mathrm{amp}}(\omega)$ and $T_{\mathrm{hyd}}(\omega)$ represent the transfer functions of the amplifier and hydrophone, respectively.

The simulated and measured transmit transfer functions, in water, for the fabricated linear array are shown in Fig. 8. A shift of $\approx 0.2\,\mathrm{MHz}$ between the resonance peaks occurs, which may be due to a several practical factors, such as the thin layers of glue used to stack all the layers of the array. Even though these layers were included in the simulations with average expected thicknesses and medium properties, in practice they could be slightly different and also vary a little bit along the aperture of the array. Moreover, some of the piezo-electric properties of the fabricated PZT may have an uncertainty up to $10\,\%$ relative to the nominal values used in simulations. However, a $\pm 10\,\%$ change in resonance frequency as a result of the uncertainty in the thickness or the elastic properties would still only explain about $\pm 0.12\,\mathrm{MHz}$ of the shift. Therefore, not all of the difference in resonance frequency between simulations and experiments can be explained by the uncertainty of the properties of the PZT material. Another consideration is that the backing and/or the lead piece are not made of standardized materials, therefore, their acoustic properties probably differed from those used in simulations.

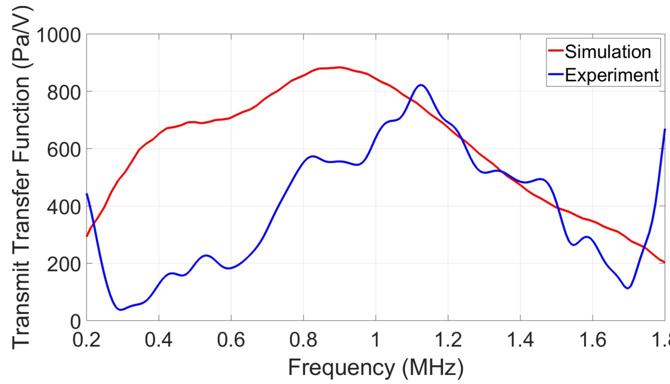

Figure 8: Measured and simulated transmit transfer function, in water, of the prototype linear transducer array of Fig. 7.

The wavefield used to compute the transmit transfer function of Fig. 8 was measured near the natural focus in elevation (i.e. $z_0 = 113.5\,\mathrm{mm}$), instead of in the far field, as is usually applied for medical imaging probes. This was done because of the relatively large focal distance of the array combined with the limited dimensions of the water tank in which the measurements were carried out. Therefore, the diffraction correction term, which transforms the pressure measured by the hydrophone (i.e. at $z_0 = 113.5\,\mathrm{mm}$) to the pressure at the transducer surface, and which was computed using Field II [28], [29] and cross-checked with other simulation tools, resulted to have a spike-like shape that finally resulted in the curve observed in Fig. 8. However, around resonance, the measured magnitudes of transmit efficiency ($0.81\,\mathrm{kPa/V}$) corresponded reasonably well with the simulations ($0.88\,\mathrm{kPa/V}$). In contrast, one of the more efficient ultrasound transducer arrays reports, at resonance, a value of $\approx 20\,\mathrm{kPa/V}$ in water [30], however, if placed in a clamp-on configuration (see Fig. 1b or Fig. 2a), the high reflection coefficient of the water - pipe wall interface in combination with the reflection coefficient of the coupling piece - pipe wall interface would reduce its efficiency in water to $\approx 1.2\,\mathrm{kPa/V}$, ultimately comparable to the measured values shown in Fig. 8. The bandwidth of the input signal used to measure the blue curve in

This article has been accepted for publication in IEEE Transactions on Ultrasonics, Ferroelectrics, and Frequency Control. This is the author's version which has not been fully edited and content may change prior to final publication. Citation information: DOI 10.1109/TUFFC.2022.3186170

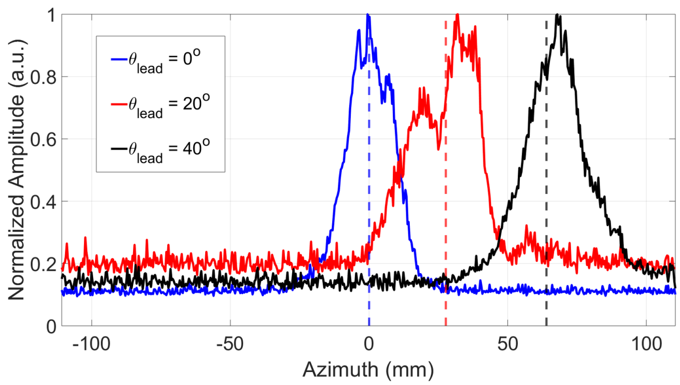

Figure 9: Measured linear scans of the amplitude of the acoustic wavefield in water, generated by the transducer array of Fig. 7 for three different beam steering angles in lead. The dashed vertical lines indicate the theoretical expected position of the peak pressures for the theoretical sounds speeds involved.

Fig. 8 ranged approximately between $0.2\,\mathrm{MHz}$ and $1.7\,\mathrm{MHz}$, which means that outside of this bandwidth the energy of the excitation signal drops down faster than that of the received signal, i.e. $V_{\text{tr}}(\omega)$ in Eq. 1 tends to zero, resulting in the observed increase of the Transmit Transfer Function outside of this bandwidth.

C. Beam Steering and Wave Mode Conversion

In the experimental setup, time delays were applied to the array elements to steer an acoustic beam through the lead coupling piece, the metal layer representing the pipe wall, and finally into the water, where a linear scan of the wavefield was performed at a depth of $z_0 = 113.5\,\mathrm{mm}$ and along the azimuthal direction of the array.

Three steering angles in lead were tested: $\theta_{\text{lead}} = 0°$, $\theta_{\text{lead}} = 20°$ and $\theta_{\text{lead}} = 40°$. Given the compressional bulk wave sound speed of lead ($c_L = 2200\,\mathrm{m/s}$) and stainless steel ($c_L = 5800\,\mathrm{m/s}$), Snell's law predicts a critical angle of $22\,°$, beyond which only shear waves will propagate in the pipe wall. Therefore, for the steering angle of $40\,°$, the shear bulk wave speed of stainless steel ($c_T = 3100\,\mathrm{m/s}$), was used. Fig. 9 shows the measured linear scans. As expected, the peak pressure shifts as a function of the steering angle. Furthermore, given the measured azimuthal location $x_{\max}$ of the main peak of a linear scan profile and the associated time signal from which the transit time t_{w} of the acoustic beam can be extracted, the steering angle of the acoustic beam in water ($c_{\text{w}} = 1500\,\mathrm{m/s}$) was determined from

$$\theta_{\text{w}} = \arcsin\left(\frac{x_{\max}}{c_{\text{w}} t_{\text{w}}}\right). \tag{2}$$

For the considered angles $\theta_{\text{lead}} = 20\,°$ and $\theta_{\text{lead}} = 40\,°$, the measured angles in water were $\theta_{\text{w}} = 15.8\,°$, and $\theta_{\text{w}} = 30.6\,°$, respectively. These were comparable to the theoretical values of $\theta_{\text{w}} = 13.2\,°$, and $\theta_{\text{w}} = 25.4\,°$. The discrepancies are most likely due to the sound speeds considered in the theoretical calculations. Other evidence was the constant offset between the theoretical and measured peak locations for each considered angle. At $\theta_{\text{lead}} = 20\,°$, an interference effect was observed between the bulk compressional and shear waves in the steel, which refracted into the water with a similar angle and produced the dip in the amplitude measured in the azimuthal range between $20 - 30\,\mathrm{mm}$. The results of Fig. 9 confirmed that, with the fabricated array, it is possible to also excite shear waves in the pipe wall and measure flow with either scenario Fig. 6a or scenario Fig. 6b.

Noise floor levels are slightly different for each scan in Fig. 9 because, in each case, particular wave interferences were occurring, which lead to measurement of a slightly different peak amplitude for normalization.

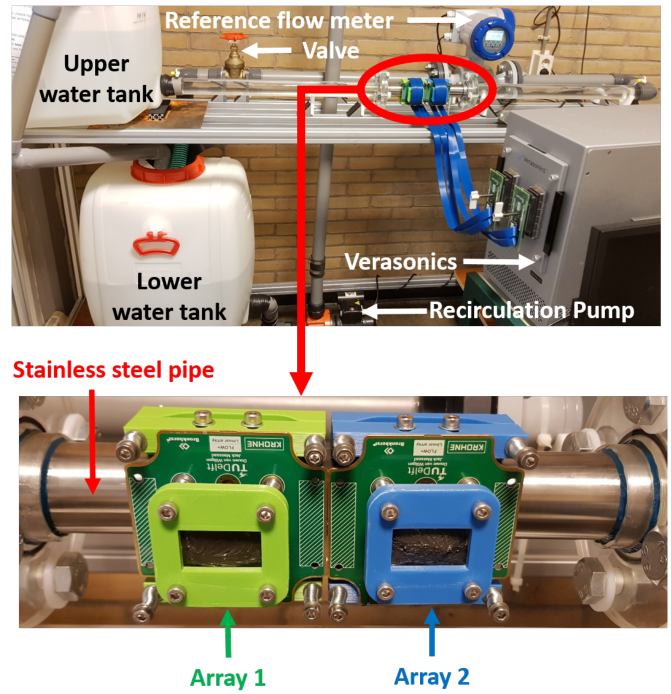

Figure 10: Custom-made flow loop to perform clamp-on ultrasonic flow measurements with our fabricated prototype arrays. The red oval indicates the location of the flow sensor with the two linear arrays (top figure). Gravity was used to drive flow from left to right through the stainless steel pipe section on which the arrays were installed (bottom figure). The custom-made 3D-printed green and blue frames were designed with a system of screws and springs to achieve mechanical coupling of the backing with the PCB (front screws), and of the lead coupling piece (not visible here) with the pipe wall (back screws).

VI. Flow Speed Measurements

In this section it is shown how the fabricated linear arrays were used to measure flow, and how new tools and techniques can be implemented to achieve more precise flow measurements.

A. Setup

A custom-made, gravity-driven flow loop was built, see Fig. 10. It mainly consisted of PVC pipes with a constant inner diameter of $40\,\mathrm{mm}$, and contained a reference in-line ultrasonic flow meter (Optosonics 3400, KROHNE Nederland B.V., Dordrecht, NL). The liquid used was water. The flow rate was manually controlled with a valve. With this setup it was possible to achieve flow speeds of water up to $0.6\,\mathrm{m/s}$ for up to $15\,\mathrm{min}$.

A $30\,\mathrm{cm}$ long section consisted of a 304 stainless steel pipe ($c_L = 5920\,\mathrm{m/s}$, $c_T = 3141\,\mathrm{m/s}$), with a wall thickness of $h = 1\,\mathrm{mm}$ and an inner diameter of $D = 40\,\mathrm{mm}$. Both fabricated linear arrays were centrally clamped on this pipe section via custom-made 3D-printed frames to ensure mechanical coupling with the pipe. As can also be seen in Fig. 10, the arrays were not clamped on the top of the pipe but rather at a sideway location to avoid the potential non-reciprocal effects of bubbles on the measurements.

The axial transducer separation was $80\,\mathrm{mm}$ (see Fig. 6c), and the flow speed of water ($c_{\text{liquid}} = 1500\,\mathrm{m/s}$) was measured in both scenarios. For compressional waves in the pipe wall, the required steering angle was $12.85\,°$, and the desired wave mode (see Fig. 6a) was expected to arrive at $\approx 350\,\mu\mathrm{s}$. For shear waves in the pipe wall, the steering angle of the acoustic beam within the lead piece was $32.75\,°$, and the desired wave mode (Fig. 6b) was expected to arrive at $\approx 130\,\mu\mathrm{s}$. These transit times were also cross-checked with FEM simulations.

B. Data Acquisition

Two custom-made PCBs were designed to wire out each piezo-element of both linear arrays to a Verasonics Vantage 256 system. This machine was used to excite the piezo-elements with a 1-cycle square pulse with a center frequency of $f_c = 1\,\mathrm{MHz}$ and a peak voltage of $5\,\mathrm{V}$. Time delays in transmission were also implemented with this machine to produce steered acoustic beams.

Measurements with different pairs of piezo-elements confirmed that the Verasonics machine kept the timing of the signals stable enough to perform flow measurements. The time jitter of the machine was reported to be $\approx 4\,\mathrm{ps}$, which was an acceptable value given the few tens of nanoseconds of the expected transit time differences to be measured with our setup.

Upstream and downstream measurements were performed in an interleaved fashion to minimize the effects of temperature change on the sound speed of the liquid, and therefore on the flow speed estimates. One thousand measurements were performed in each direction, with a pulse repetition frequency (PRF) of $\approx 87\,\mathrm{Hz}$. This allowed the recording of all measurements in $23\,\mathrm{s}$. Element signals were recorded with a sampling frequency of $62.5\,\mathrm{MHz}$. Finally, all signals were exported for further processing.

C. Data Processing Sequence

For each flow speed, the signals were processed as shown in the flowchart of Fig. 11. The bandpass filter applied to the raw signals consisted of a 5^{th}-order Butterworth filter. Furthermore, one of the arrays turned out to have 9 broken elements. The signals corresponding to these elements were removed from the analysis, as well as the signals corresponding to their mirror counterparts from the other array.

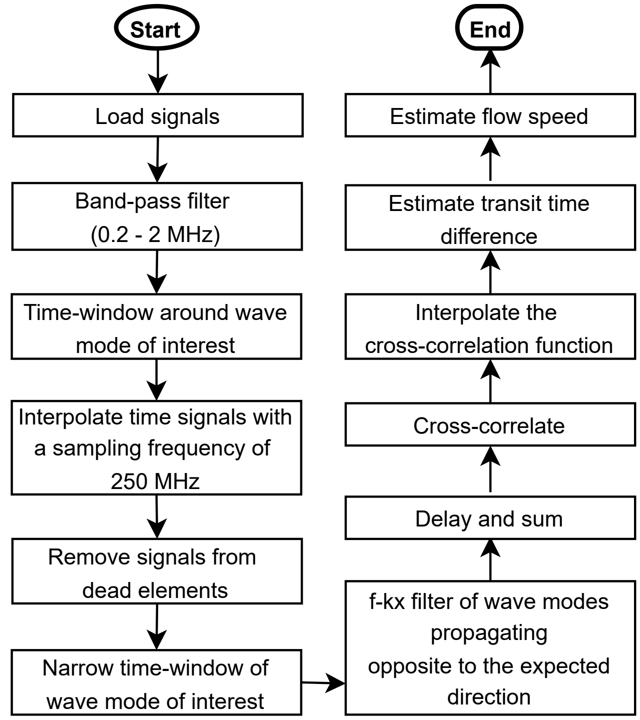

Figure 11: Signal processing sequence applied to the measured signals from the flow sensor of Fig. 10.

A particularly powerful new tool that linear arrays bring into ultrasonic flow metering is the possibility to filter out undesired spurious wave modes. Given the recorded signals of several transducer elements, it is possible to visualize the propagating wave modes, both in the space-time (x-t) domain and, after applying a 2D Fourier transformation, in the frequency-wavenumber (f-k_x) domain. Although the wave modes could be identified in the time domain, it may not always be possible to easily isolate the desired wave mode because it may overlap with the undesired ones. The probability of this overlap increases when the transducers are installed closer to each other, and also when the sensor is installed nearby other features of the pipeline, such as flanges and/or valves. However, the direction (i.e. steering angle) of the transmitted beam is always known during ultrasonic flow metering. Therefore, the expected direction from which it should arrive is also known, and will correspond with a specific straight line in the f-k_x domain. Thus, with linear arrays, this wave mode may be identified in the f-k_x domain, and all other undesired wave modes may be filtered-out, including guided waves and reflections, to finally obtain cleaner time signals to estimate the flow speed.

Lastly, the signals corresponding to each individual receiving element are delayed to align the signals for a given beam direction, and these are subsequently summed altogether. The obtained signals from an upstream and a downstream measurement are subsequently cross-correlated to obtain their transit time difference. This was finally used as input, together with the properties of the pipe and the liquid, to estimate the flow speed.

D. Flow Speed Measurements

Considering a sound speed in water of $c_{\text{liquid}} = 1500\,\text{m/s}$, it was possible to compute the theoretical transit time difference Δt between upstream and downstream signals measured for the travel paths in the scenarios of Fig. 6a and Fig. 6b. At zero-flow conditions (in which theoretically $\Delta t = 0\,\text{ns}$ for both scenarios), values of $\Delta t = 0.55\,\text{ns}$ and $\Delta t = 0.19\,\text{ns}$ respectively, were measured for the scenarios of Fig. 6a and Fig. 6b. Furthermore, a median absolute deviation of $\text{mad} = 2.19\,\text{ns}$ and $\text{mad} = 1.06\,\text{ns}$, respectively, was found. For the highest possible reference flow speed, i.e. $v_{\text{ref}} = 0.6\,\text{m/s}$, theoretical transit time differences of $\Delta t = 39.27\,\text{ns}$ and $\Delta t = 33.86\,\text{ns}$, respectively, were computed. The measured values for this flow speed were $\Delta t = 38.46\,\text{ns}$ and $\Delta t = 33.80\,\text{ns}$, with median absolute deviation of $\text{mad} = 4.05\,\text{ns}$ and $\text{mad} = 2.39\,\text{ns}$, respectively, see Fig. 12. The slight discrepancies between measured and theoretical values are probably due to the chosen theoretical sound speed of the water. Also, when considering compressional waves in the pipe wall, the transit time of the acoustic waves is higher than with shear waves, which is the reason for the higher transit time differences in the former scenario relative to the latter.

Other beams, corresponding to different travel paths than those shown in Fig. 6a and Fig. 6b, were also recorded. However, their associated amplitudes were lower than for the intended ones because their arrival position deviated from the $80\,\text{mm}$ axial transducer separation.

The flow speed v_{f} can be obtained from the acoustic beam path, the properties of the pipe, the sound speed of the liquid, and the measured transit time differences between upstream and downstream measurements. This requires computing the positive root of the following second-order equation

$$[\Delta t \sin^2(\theta_{\text{liquid}})]v_{\text{f}}^2 + [4bD\tan(\theta_{\text{liquid}})]v_{\text{f}} - \Delta t c_{\text{liquid}}^2 = 0, \quad (3)$$

where θ_{liquid} represents the steering angle of the acoustic beam in the liquid, and b represents the number of bounces (v-shapes) of the acoustic beam within the pipe wall before arriving at the receiving transducer. Eq. 3 assumes that the flow speed can be sufficiently described by its average speed, and does not take into account flow regime effects such as turbulent vs. laminar flow.

Figure 13 shows all measured flow speeds and their respective uncertainty. Similar to Fig. 12, measurement uncertainty increases with the flow speed, which is due to increasing flow turbulence. For the measurement scenarios of Fig. 6a and Fig. 6b, the flow speed was obtained and compared with the reference measurement. At zero-flow conditions, flow speeds of $v_{\text{f}} = 0.008\,\text{m/s}$ and $v_{\text{f}} = 0.003\,\text{m/s}$, were obtained, with a median absolute deviation of $\text{mad} = 0.03\,\text{m/s}$ and

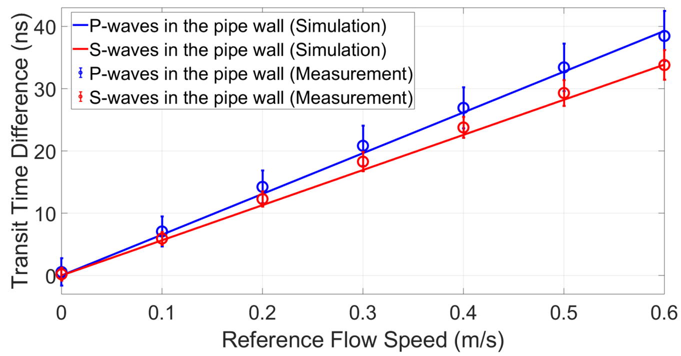

Figure 12: Theoretical transit time difference (solid lines) and measured transit time difference (circles) between upstream and downstream signals, versus flow speed, for the scenarios of Fig. 6a (blue) and Fig. 6b (red). Vertical bars indicate median absolute deviations.

$\text{mad} = 0.02\,\text{m/s}$, respectively. Furthermore, at a reference flow speed of $v_{\text{ref}} = 0.6\,\text{m/s}$, the measured flow speeds with our prototype were $v_{\text{f}} = 0.59\,\text{m/s}$ and $v_{\text{f}} = 0.60\,\text{m/s}$, with a median absolute deviation of $\text{mad} = 0.06\,\text{m/s}$ and $\text{mad} = 0.04\,\text{m/s}$, respectively. A linear fit between the reference flow speeds and those measured with our fabricated prototype was performed. The slopes of the linear fits shown in Fig. 13 were 0.977 and 1.006, respectively, which suggest a good correspondence between reference and measurements.

To compute the flow speeds reported above, a nominal value of $c_{\text{liquid}} = 1500\,\text{m/s}$ was used for water at room temperature (i.e. $24\,°\text{C}$), which ultimately affects the accuracy of the obtained flow speed values, thus highlighting the importance of monitoring c_{liquid}. This could be done dynamically by e.g. using a transducer array to transmit a perpendicular acoustic beam and perform a pulse-echo measurement, identify the transit time of the signal reflected from the liquid-pipe interface opposite to the transducer location, and use it to finally compute c_{liquid}. [7]

Given the water filled pipe with $40\,\text{mm}$ pipe inner diameter, all measured non-zero flow speeds shown in Fig. 13 had an associated Reynolds number $Re > 2500$, thus measurements were always conducted in the turbulent flow regime. In addition, the pipe section on which the sensors were placed was located far away from a bend or an entrance (see Fig. 10), such that the flow profiles could be expected to be symmetric and the boundary layers fully developed for all measured flows. This is visible in the results by the fact that no sudden jumps or an apparent change in slope as a function of the measured flow speeds are visible in Fig. 13.

VII. Discussion

The acoustic characterization results of our first linear array prototype, in particular those shown in Fig. 8 and Fig. 9, provided confidence in the design of our future matrix array. The observed differences in resonance peaks may be attributed to differences in simulated and actual dimensions of the layers of the arrays, as well as to differences between simulated and actual piezo-electric properties of the PZT, which may differ by up to $10\,\%$.

This article has been accepted for publication in IEEE Transactions on Ultrasonics, Ferroelectrics, and Frequency Control. This is the author's version which has not been fully edited and content may change prior to final publication. Citation information: DOI 10.1109/TUFFC.2022.3186170

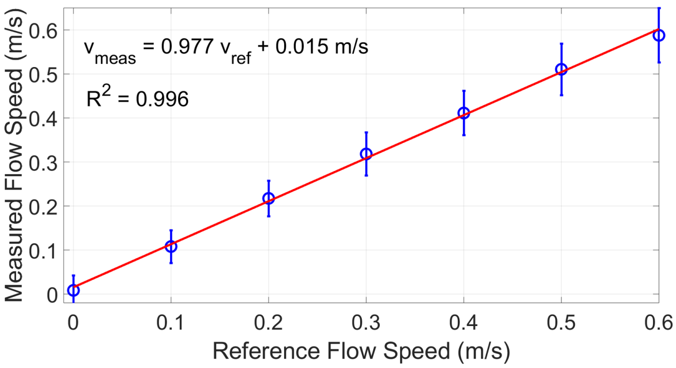

(a)

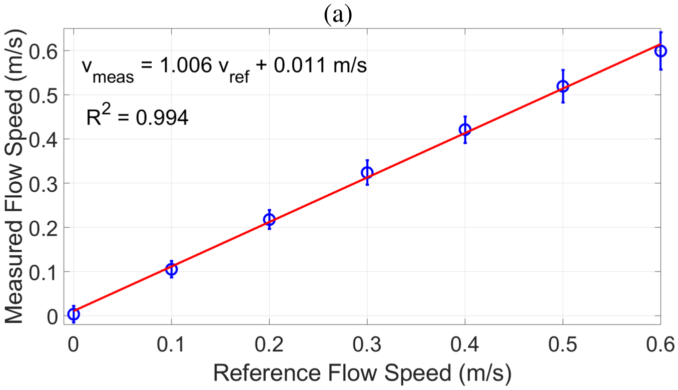

(b)

Figure 13: Measured versus reference flow speed of water for the acoustic beam paths of (a) Fig. 6a and (b) Fig. 6b. Vertical bars indicate median absolute deviations.

The pitch of our array ensures sufficiently dense spatial sampling of Lamb waves in pipes with wall thicknesses up to $5\,\mathrm{mm}$. Furthermore, the linear scan profiles in Fig. 9 demonstrated its beam steering capabilities. The performed flow measurements also give confidence in the use of transducer arrays for flow measurement. A clear benefit of using matrix arrays lies in achieving automatic beam alignment and the possibility of measuring the parameters of the pipe and the fluid.

The region of low SNR predicted in Fig. 3a for liquids with relatively high attenuation may be narrowed down in two simple ways. First, the steering angle of the beam could be decreased and the acoustic beam could bounce less often within the pipe, resulting in less reflection losses and propagation losses, and thus increasing SNR. Second, the beam steering angle could be increased enough to operate the sensor in the shear wave mode shown in Fig. 6b. Of course, the input voltage may also be increased to achieve higher SNRs. However, for devices with a commercial purpose, the standard IEC 60079-11 is considered, which states the maximum allowable energy emission of the device to ensure its intrinsic (explosion) safety, and ultimately sets its maximum input voltage to $5\,\mathrm{V}$.

Flow speeds measured by using compressional waves in the pipe wall were comparable, in terms of uncertainty, to those measured by using shear waves in the pipe wall (Fig. 13). In terms of SNR, the amplitudes of the time signals measured using compressional waves in the pipe wall were $\approx 1.7\,\mathrm{dB}$ lower than the amplitudes of the time signals measured using shear waves in the pipe wall. This should be compared to the $\approx 3.3\,\mathrm{dB}$ expected SNR difference from the theoretical calculations for water ($\alpha = 0.002\,\mathrm{dB/MHz.cm}$) shown in Fig. 3. Moreover, calculations such as those in Fig. 3 would allow to decide whether to operate the flow sensor by using either compressional or shear waves in the pipe wall. The travel paths for the former are usually much longer than for the latter, which would therefore be more preferable for measuring the flow speed of highly attenuating liquids or gases. Compressional waves in the pipe wall could be used when the length of the pipe section in which the sensor would be installed is very limited and only relatively small beam steering angles are possible.

The results shown in Fig. 13 demonstrate the correct performance of our proposed sensor, and that the goal of our paper to show the concept of array-based clamp-on ultrasonic flow meters was achieved. The Verasonics machine used to drive the transducers and digitize the signals operates within a $4\,\mathrm{ps}$ time jitter, which was decided to be enough to measure the nanosecond transit time differences shown in Fig. 12. Furthermore, amplitude jitter of this machine depended on TGC gain and PGA and LNA amplifier settings. At their maximum values, the measured noise floor of the Verasonics was approximately $28\,\mu\mathrm{V_{RMS}}$. During flow measurements, these amplification settings allowed to measure amplitudes well above ($+60\,\mathrm{dB}$) the amplitude jitter. However, the entire flow metering system is not yet optimized to achieve maximum measurement performance. The actual parameters of the pipe and the liquid used as input in Eq. 3 were not measured. Instead, nominal values were used, and these probably deviate from the real ones. Future matrix transducer arrays should be able to measure pipe and liquid parameters prior to flow metering [6], [7], improving measurement accuracy. Furthermore, relatively low excitation voltages in combination with a single-cycle rectangular excitation pulse resulted in low acoustic pressures. However, the per-channel SNR of the flow-sensitive wave mode was approximately $30\,\mathrm{dB}$, and commercial ultrasonic flow meters are known to operate with SNRs as low as $20\,\mathrm{dB}$. The noise floor in the measurements was dominated by the thermal noise of the amplifiers of the Verasonics machine, which is higher than the noise floor levels of typical ultrasonic flow metering systems because this machine is mainly used for imaging applications. All these factors contributed to the total noise level of the measurement, with the thermal noise of the piezo-elements not being dominant anymore. Thus, at this point, a comparison between our sensor and standard clamp-on flow meters would not be fair, and is also not the goal of this work. Therefore, future research will be focused on implementing several techniques to achieve a more fair comparison with current sensors, such as using higher input voltages in combination with modulated signals (e.g. long linear chirp, coded excitation) [31], adding a matching circuit or buffer amplifiers to better match the transducers and the Verasonics machine electrically, as well as using a low-noise application-specific integrated circuit (ASIC) to drive and read-out the signals from the piezo-elements.

This article has been accepted for publication in IEEE Transactions on Ultrasonics, Ferroelectrics, and Frequency Control. This is the author's version which has not been fully edited and content may change prior to final publication. Citation information: DOI 10.1109/TUFFC.2022.3186170

Even for a symmetric flow profile, measuring flow speed with a single travel path (i.e. either the one shown in Fig. 6a or in Fig. 6b), does not make it possible to reconstruct the flow profile, but just to obtain a mean flow speed value. Furthermore, if the flow profile is non-symmetric, the interpretation of the measured flow speed as a mean value is flawed. With matrix arrays, beam steering would also be possible along the circumferential direction. This would allow to generate different acoustic beams that would propagate through different star-shaped travel paths, making it possible to extract information about the flow profile. At the moment, this is an active topic of research.

In principle, acoustic paths that differ from those depicted in Fig. 6 are also present, e.g. the 5 or 7 bounce versions of the path in Fig. 6a. The acoustical signals that travel along these paths are also sensitive to flow and will also arrive at the receiving transducer. As shown in [32], these signals could be used to extract more estimates of the flow speed. However, these beams have a different travel path compared to the beams shown in Fig. 6, which means that their beam width at the moment of arrival would not be optimal anymore to achieve the maximum SNR as determined in [8].

VIII. Conclusion

In this work, the detailed rationale of the acoustic design of a clamp-on ultrasonic flow meter based on two matrix transducer arrays was presented. Moreover, a proof-of-concept prototype based on two linear arrays was fabricated and characterized on three critical aspects: efficiency, beam steering and wave mode conversion. Furthermore, the prototype was successfully used to measure the flow speed of water flowing through a $40\,\mathrm{mm}$-inner diameter stainless steel pipe. With electronic beam steering, it was possible to measure flow speed in two modalities: using compressional and shear waves in the pipe wall. For both measurement modalities, the correlation factor between reference and measured flow speed was > 0.994.

Appendix A

A. Relevant Elastic and Electrical Properties of Materials

For the Finite Element simulations, the compressional bulk wave sound speed (c_L), shear bulk wave sound speed (c_T), density (ρ), and attenuation coefficient at a resonance frequency of $1\,\mathrm{MHz}$ (α) were defined. The parameters reported in Table I were used for the non-PZT materials. Applied mechanical and electrical properties of the PZT materials HK1HD and PZ26 are reported in Table II.

B. Final Geometries of Materials

The geometries of the designed acoustic stack shown in Fig. 2a are shown in Table III. For the PZT materials (HK1HD for the matrix array, and PZ26 for the linear array), an elevation dimension had to be defined for calculations of electrical impedance. For HK1HD and PZ26, this dimension was $0.62\,\mathrm{mm}$ (yielding square elements for the matrix array) and $12\,\mathrm{mm}$ (giving rectangular elements for the linear array), respectively.

Table I: Elastic properties of the layers used in FEM simulations for designing the acoustic stack of the matrix transducer array shown in Fig. 2a: compressional bulk wave sound speed (c_L), shear bulk wave sound speed (c_T), density (ρ), and attenuation coefficient (α).

Layer	Elastic Properties			
	c_L (m/s)	c_T (m/s)	ρ (kg/m^3)	α (dB/MHz.cm)
Backing	3602	2396	1850	5
PCB	3602	2396	1850	0.46
Copper	5010	2270	8930	0.4
Lead	2200	700	11200	0
Stainless Steel	5800	3100	7900	0.3
Water	1496	-	1000	0.002

Table II: Electrical and mechanical properties of PZT materials HK1HD and PZ26 used in FEM simulations for designing the acoustic stack of the matrix transducer array shown in Fig. 2a: dielectric constant (ϵ_{33}), coupling factor ($\mathrm{k_{33}}$), mechanical quality factor at $1\,\mathrm{MHz}$ (Q), density (ρ), and stiffness coefficients ($\mathrm{c_{ij}}$).

Parameter	HK1HD	PZ26
ϵ_{33}	2755	700
$\mathrm{k_{33}}$ (a.u.)	0.75	0.68
Q	120	776
ρ (kg/m^3)	8000	7700
$\mathrm{c_{11}}$	157	168
$\mathrm{c_{33}}$	137	123
$\mathrm{c_{44}}$	22	30.1
$\mathrm{c_{12}}$	100	110
$\mathrm{c_{13}}$	105	99.9
$\mathrm{c_{66}}$	28	28.8

Table III: Dimensions of the layers forming the acoustic stack shown in Fig. 2a.

Simulated Geometries		
Layer	**Thickness (mm)**	**Width (mm)**
Backing	40	45
PCB	1.6	60
HK1HD (PZ26)	1.24 (1.67)	0.62
Copper	0.02	26
Lead	11	60

Furthermore, Table IV reports the geometry of the fabricated linear arrays for the proof-of-concept prototype. Length refers to the dimension in the circumferential direction.

Table IV: Dimensions of the layers forming the fabricated linear arrays used as proof-of-concept.

Fabricated Geometry			
Layer	**Thickness (mm)**	**Width (mm)**	**Length (mm)**
Backing	13	45	12
PCB	1.6	60	60
PZ26	1.67	0.62	12
Copper	0.02	26	12
Lead	11	60	40

Acknowledgment

This work is part of the research programme FLOW+, which is financed by the Dutch Technology Foundation STW (project

15031) and industrial partners Bronkhorst and KROHNE.

References

[1] R. C. Baker, *Flow measurement handbook: industrial designs, operating principles, performance, and applications*. Cambridge University Press, 2005.

[2] W.-S. Cheung, H.-S. Kwon, K.-A. Park, and J.-S. Paik, "Acoustic flowmeter for the measurement of the mean flow velocity in pipes," *J. Acoust. Soc. Am.*, vol. 110, no. 5, pp. 2308–2314, 2001.

[3] J. Wendoloski, "On the theory of acoustic flow measurement," *J. Acoust. Soc. Am.*, vol. 110, no. 2, pp. 724–737, 2001.

[4] D. Kurniadi and A. Trisnobudi, "A multi-path ultrasonic transit time flow meter using a tomography method for gas flow velocity profile measurement," *Part. Part. Syst. Charact.*, vol. 23, no. 3-4, pp. 330–338, 2006.

[5] M. Sanderson and H. Yeung, "Guidelines for the use of ultrasonic non-invasive metering techniques," *Flow. Meas. Instrum.*, vol. 13, no. 4, pp. 125–142, 2002.

[6] J. Massaad, P. L. M. J. van Neer, D. M. van Willigen, M. A. P. Pertijs, N. de Jong, and M. D. Verweij, "Towards a calibration-free ultrasonic clamp-on flow meter: Pipe geometry measurements using matrix arrays," in *Proc. Meet. Acoust.*, vol. 39, no. 1. Acoustical Society of America, 2019, p. 065001.

[7] J. Massaad, P. L. Van Neer, D. M. Van Willigen, A. Sabbadini, N. De Jong, M. A. Pertijs, and M. D. Verweij, "Measurement of pipe and fluid properties with a matrix array-based ultrasonic clamp-on flow meter," *IEEE Trans. Ultrason. Ferroelectr. Freq. Control*, vol. 69, no. 1, pp. 309–322, 2021.

[8] J. Massaad, P. L. M. J. van Neer, D. M. van Willigen, M. A. P. Pertijs, N. de Jong, and M. D. Verweij, "Suppression of lamb wave excitation via aperture control of a transducer array for ultrasonic clamp-on flow metering," *J. Acoust. Soc. Am.*, vol. 147, no. 4, pp. 2670–2681, 2020.

[9] F. Hofmann, "Fundamentals of ultrasonic-flow measurement for industrial applications," *KROHNE Messtechnik GmbH & Co. KG, Duisburg*, pp. 1–31, 2000.

[10] D. Ito, H. Kikura, M. Aritomi, and M. Mori, "Application of an ultrasonic array sensor to air-water bubbly flow measurement," in *Journal of Physics: Conference Series*, vol. 147, no. 1. IOP Publishing, 2009, p. 012005.

[11] A. Jäger, A. Unger, H. Wang, Y. Arnaudov, L. Kang, R. Su, D. Lines, S. N. Ramadas, S. Dixon, and M. Kupnik, "Ultrasonic phased array for sound drift compensation in gas flow metering," in *2017 IEEE International Ultrasonics Symposium (IUS)*. IEEE, 2017, pp. 1–4.

[12] L. Kang, A. Feeney, and S. Dixon, "Flow measurement based on two-dimensional flexural ultrasonic phased arrays," in *Proceedings of Meetings on Acoustics 6ICU*, vol. 32, no. 1. Acoustical Society of America, 2017, p. 045012.

[13] L. Kang, A. Feeney, R. Su, D. Lines, A. Jäger, H. Wang, Y. Arnaudov, S. N. Ramadas, M. Kupnik, and S. Dixon, "Two-dimensional flexural ultrasonic phased array for flow measurement," in *2017 IEEE International Ultrasonics Symposium (IUS)*. IEEE, 2017, pp. 1–4.

[14] X. Chen, C. Liu, D. Yang, X. Liu, L. Hu, and J. Xie, "Highly accurate airflow volumetric flowmeters via pmuts arrays based on transit time," *Journal of Microelectromechanical Systems*, vol. 28, no. 4, pp. 707–716, 2019.

[15] C. Haugwitz, A. Jäger, G. Allevato, J. Hinrichs, A. Unger, S. Saul, J. Brötz, B. Matyschok, P. Pelz, and M. Kupnik, "Flow metering of gases using ultrasonic phased-arrays at high velocities," in *2019 IEEE International Ultrasonics Symposium (IUS)*. IEEE, 2019, pp. 1129–1132.

[16] S. Peller and O. Regensburg, "Ultrasound beamforming with phased capacitive micromachined ultrasonic transducer arrays for the application flow rate measurement," *RARC 2020*, p. 161, 2020.

[17] M. Meribout, F. Shehzad, N. Kharoua, and L. Khezzar, "An ultrasonic-based multiphase flow composition meter," *Measurement*, vol. 161, p. 107806, 2020.

[18] L. Fang, Q. Zeng, F. Wang, Y. Faraj, Y. Zhao, Y. Lang, and Z. Wei, "Identification of two-phase flow regime using ultrasonic phased array," *Flow Measurement and Instrumentation*, vol. 72, p. 101726, 2020.

[19] A. Kunadt, G. Pfeifer, and W.-J. Fischer, "Ultrasonic flow meter with piezoelectric transducer arrays integrated in the walls of a fiber-reinforced composite duct," in *SENSORS, 2012 IEEE*. IEEE, 2012, pp. 1–4.

[20] A. S. Dukhin and P. J. Goetz, *Characterization of liquids, dispersions, emulsions, and porous materials using ultrasound*. Elsevier, 2017.

[21] J. Massaad, D. Van Willigen, P. Van Neer, N. De Jong, M. Pertijs, and M. Verweij, "Acoustic design of a transducer array for ultrasonic clamp-on flow metering," pp. 1133–1136, 2019.

[22] P. L. M. J. van Neer, S. Blaak, J. G. Bosch, C. T. Lancée, C. Prins, A. F. W. van der Steen, and N. de Jong, "Mode vibrations of a matrix transducer for three-dimensional second harmonic transesophageal echocardiography," *Ultrasound in medicine & biology*, vol. 38, no. 10, pp. 1820–1832, 2012.

[23] C. Adams, S. Harput, D. Cowell, T. M. Carpenter, D. M. Charutz, and S. Freear, "An adaptive array excitation scheme for the unidirectional enhancement of guided waves," *IEEE Trans. Ultrason. Ferroelectr. Freq. Control*, vol. 64, no. 2, pp. 441–451, 2016.

[24] J. Li and J. L. Rose, "Implementing guided wave mode control by use of a phased transducer array," *IEEE Trans. Ultrason. Ferroelectr. Freq. Control*, vol. 48, no. 3, pp. 761–768, 2001.

[25] K.-C. T. Nguyen, L. H. Le, T. N. Tran, M. D. Sacchi, and E. H. Lou, "Excitation of ultrasonic lamb waves using a phased array system with two array probes: Phantom and in vitro bone studies," *Ultrasonics*, vol. 54, no. 5, pp. 1178–1185, 2014.

[26] W. Zhu and J. L. Rose, "Lamb wave generation and reception with time-delay periodic linear arrays: A bem simulation and experimental study," *IEEE Trans. Ultrason. Ferroelectr. Freq. Control*, vol. 46, no. 3, pp. 654–664, 1999.

[27] P. L. M. J. van Neer, G. Matte, J. Sijl, J. M. G. Borsboom, and N. de Jong, "Transfer functions of US transducers for harmonic imaging and bubble responses," *Ultrasonics*, vol. 46, no. 4, pp. 336–340, 2007.

[28] J. A. Jensen and N. B. Svendsen, "Calculation of pressure fields from arbitrarily shaped, apodized, and excited ultrasound transducers," *IEEE Trans. Ultrason. Ferroelectr. Freq. Control*, vol. 39, no. 2, pp. 262–267, 1992.

[29] J. A. Jensen, "Field: A program for simulating ultrasound systems," in 10^{th} *Nordic-Baltic Conference on Biomedical Imaging, Vol. 4, Supplement 1, Part 1*. Citeseer, 1996b, pp. 351–353.

[30] P. L. M. J. Van Neer, G. Matte, M. G. Danilouchkine, C. Prins, F. Van Den Adel, and N. De Jong, "Super-harmonic imaging: development of an interleaved phased-array transducer," *IEEE Trans. Ultrason. Ferroelectr. Freq. Control*, vol. 57, no. 2, pp. 455–468, 2010.

[31] T. Misaridis and J. A. Jensen, "Use of modulated excitation signals in medical ultrasound. part i: Basic concepts and expected benefits," *IEEE Trans. Ultrason. Ferroelectr. Freq. Control*, vol. 52, no. 2, pp. 177–191, 2005.

[32] M. Aanes, R. A. Kippersund, K. D. Lohne, K.-E. Frøysa, and P. Lunde, "Time-of-flight dependency on transducer separation distance in a reflective-path guided-wave ultrasonic flow meter at zero flow conditions," *J. Acoust. Soc. Am.*, vol. 142, no. 2, pp. 825–837, 2017.